Nature Geoscience

Supplementary Information

for

Spatial redistribution of a globally constant marine biological carbon pump

L. Delaigue[1,2], R. Sauzède[3], O. Sulpis[4], P. W. Boyd[5], H. Claustre[2], G-J. Reichart[1,6] and M. P. Humphreys[1]

[1]Department of Ocean Systems (OCS), NIOZ Royal Netherlands Institute for Sea Research, PO Box 59, 1790 AB Den Burg (Texel), the Netherlands

[2]Sorbonne Université, CNRS, Laboratoire d'Océanographie de Villefranche, Villefranche-Sur-Mer, France

[3]Sorbonne Université, CNRS, Institut de la Mer de Villefranche, Villefranche-Sur-Mer, France

[4]CEREGE, Aix Marseille Univ, CNRS, IRD, INRAE, Collège de France, Aix-en-Provence, France

[5]Institute for Marine and Antarctic Studies, University of Tasmania, Hobart, Tasmania, Australia

[6]Department of Earth Sciences, Utrecht University, Utrecht, the Netherlands

Corresponding author: Louise Delaigue (louise.delaigue@imev-mer.fr)

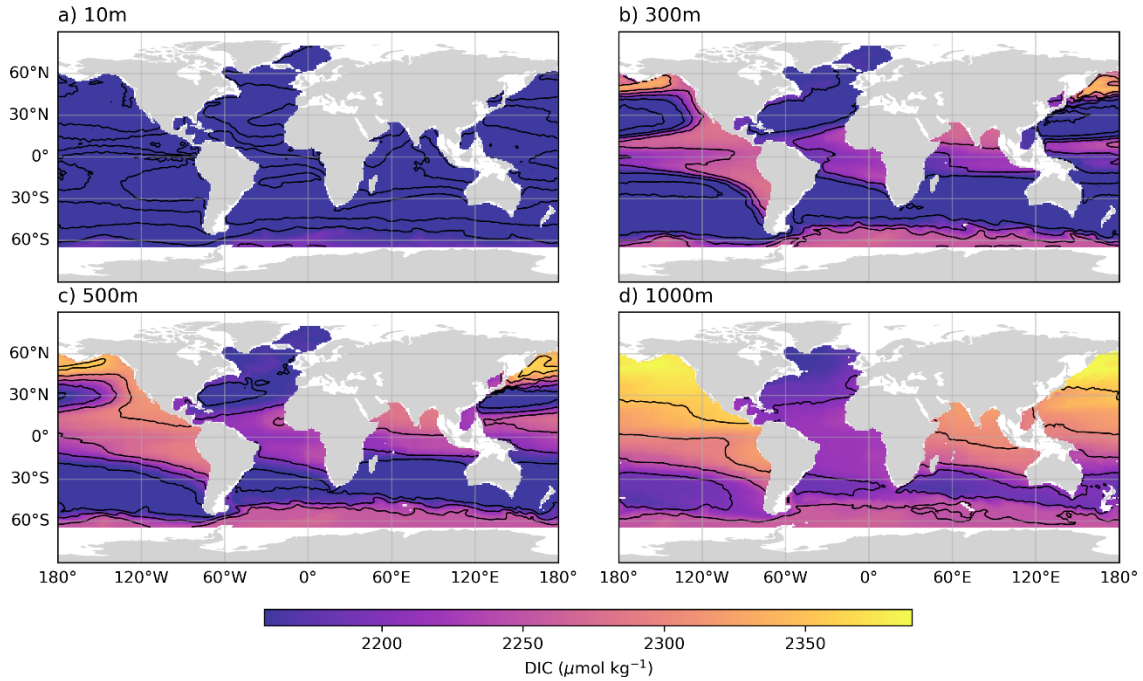

Figure S1. Annual mean DIC concentration from GCC-DIC. Four depth levels are shown: a) 10m, b) 300m, c) 500m, and d) 1000m. Black contour lines are drawn every 50 μmol kg^{-1}.

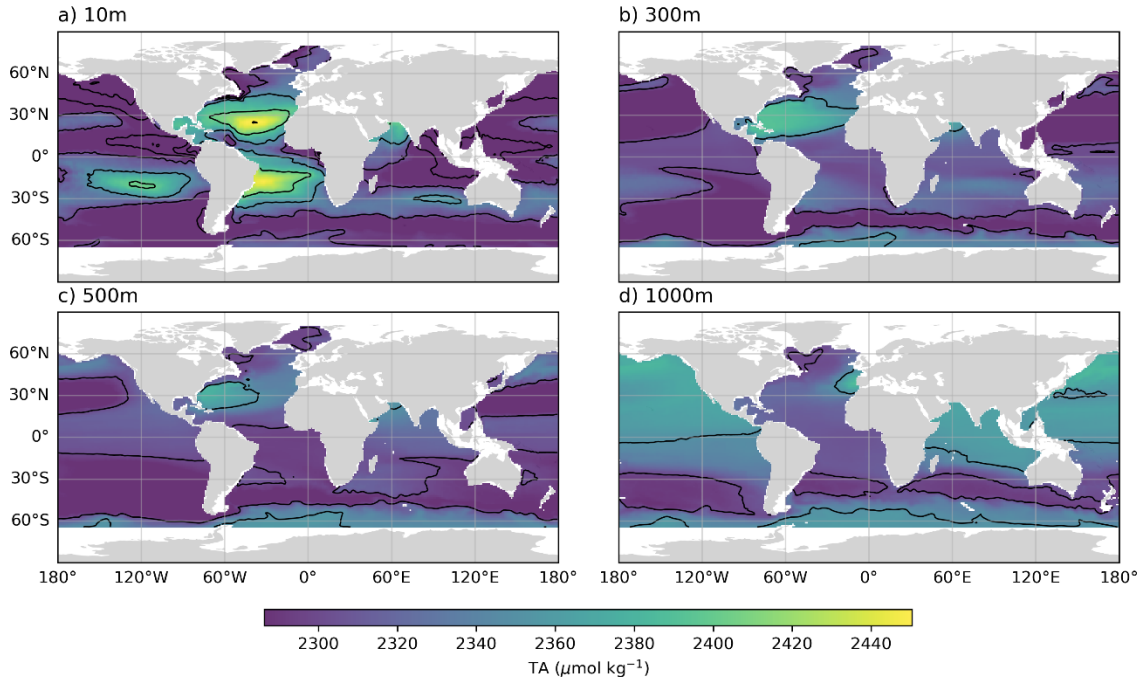

Figure S3. Annual mean TA concentration from GCC-DIC. Four depth levels are shown: a) 10m, b) 300m, c) 500m, and d) 1000m. Black contour lines are drawn every 50 µmol kg^{-1}.

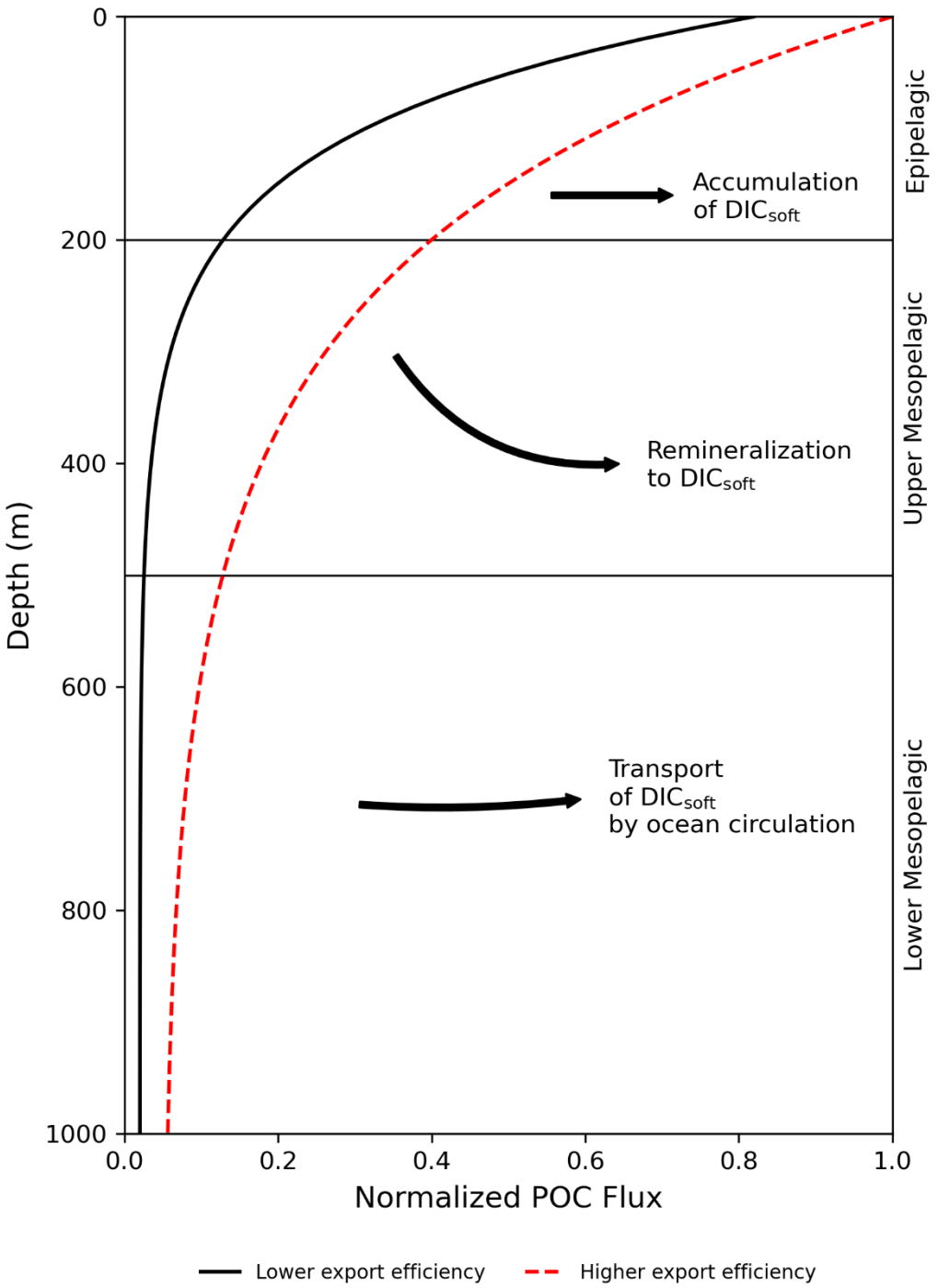

Figure S3. Conceptual schematic of the soft-tissue pump's two main fluxes and the effect of export efficiency (Frenger et al., 2024). The biological carbon pump transfers carbon from the surface to the ocean interior through the export of particulate organic carbon (POC), which is remineralized into dissolved inorganic carbon (DIC_{soft}) at depth. Higher export efficiency results in deeper remineralization, increasing the fraction of DIC_{soft} stored below the winter mixed layer and enhancing long-term carbon sequestration. DIC_{soft} accumulates at depth via remineralization (return flux) and is then redistributed laterally and vertically by ocean circulation. Environmental drivers such as stratification or shifts in phytoplankton community structure influence the export efficiency and shape the geographic pattern of sequestered DIC_{soft}.

Time-series site	Location	Time range	Temporal resolution	Bottom depth
ALOHA	22.8°N – 15.0°W	1988 – 2019	Monthly	4750m
BATS	31.67° N – 64.17° W	1988 – 2023	Monthly	5000m
CVOO	17.6°N – 24.3°W	2006 – 2019	1-3 cruises yr-1	3600m
Iceland Sea	68.0°N – 12.7°W	1985 – 2019	Seasonal	1850m
Irminger Sea	64.3°N – 28.0°W	1983 – 2019	Seasonal	1000m
K2	47.0°N – 160.0°E	1999 – 2020	1-3 cruises yr-1	6000m
KNOT	44.0°N – 155.0°E	1992 – 2020	1-3 cruises yr-1	6000m

Table S1. Key metadata of selected oceanographic time-series sites from the Synthesis Product for Ocean Time Series (SPOTS) compilation (Lange et al., 2024). The Bermuda Atlantic time series (BATS), which is not part of the compilation, was added as an additional temporal validation.

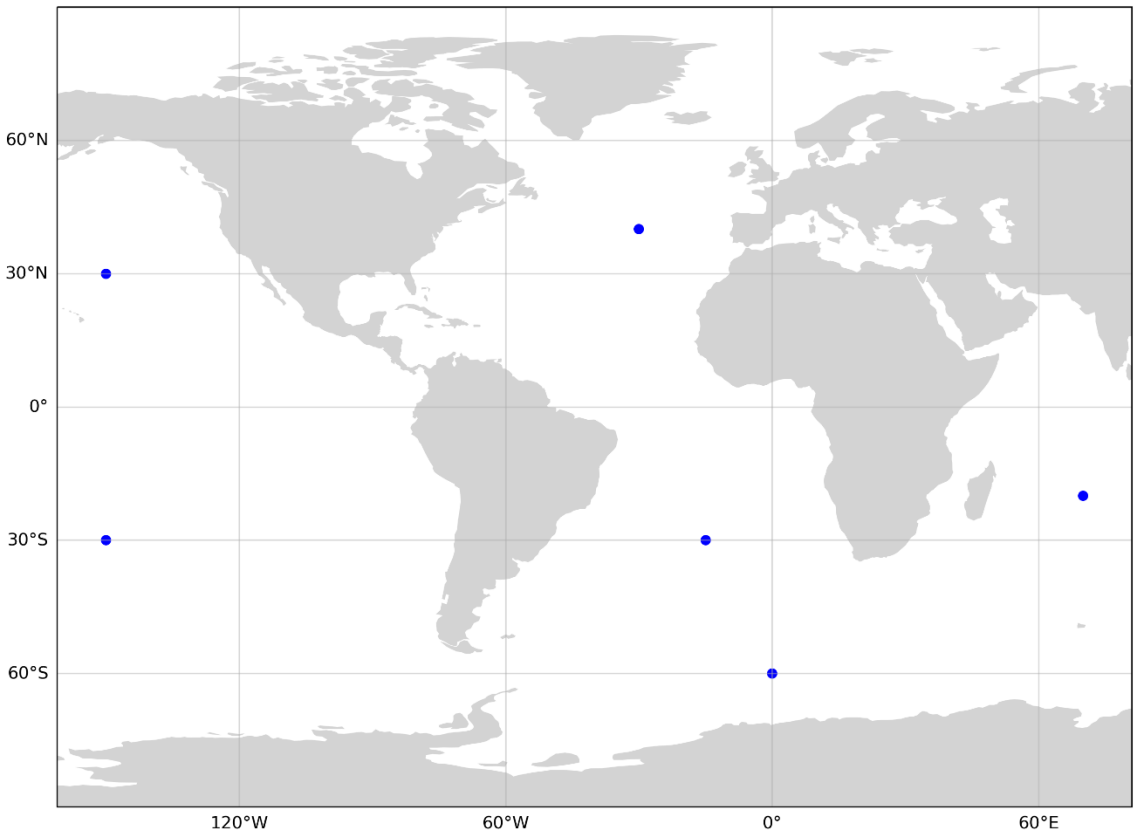

Figure S4. Locations of selected ocean basin pixels used for comparison of pressure and neutral density. Blue markers indicate representative points in the North Atlantic Ocean, South Atlantic Ocean, North Pacific Ocean, South Pacific Ocean, Indian Ocean, and Southern Ocean. These points were chosen to capture a range of oceanographic conditions across basins while keeping the analysis computationally tractable. Due to the size of the GCC-DIC dataset, it was not feasible to perform this analysis on all grid points globally; instead, representative pixels were selected to assess the pressure–neutral density relationship over time in each basin.

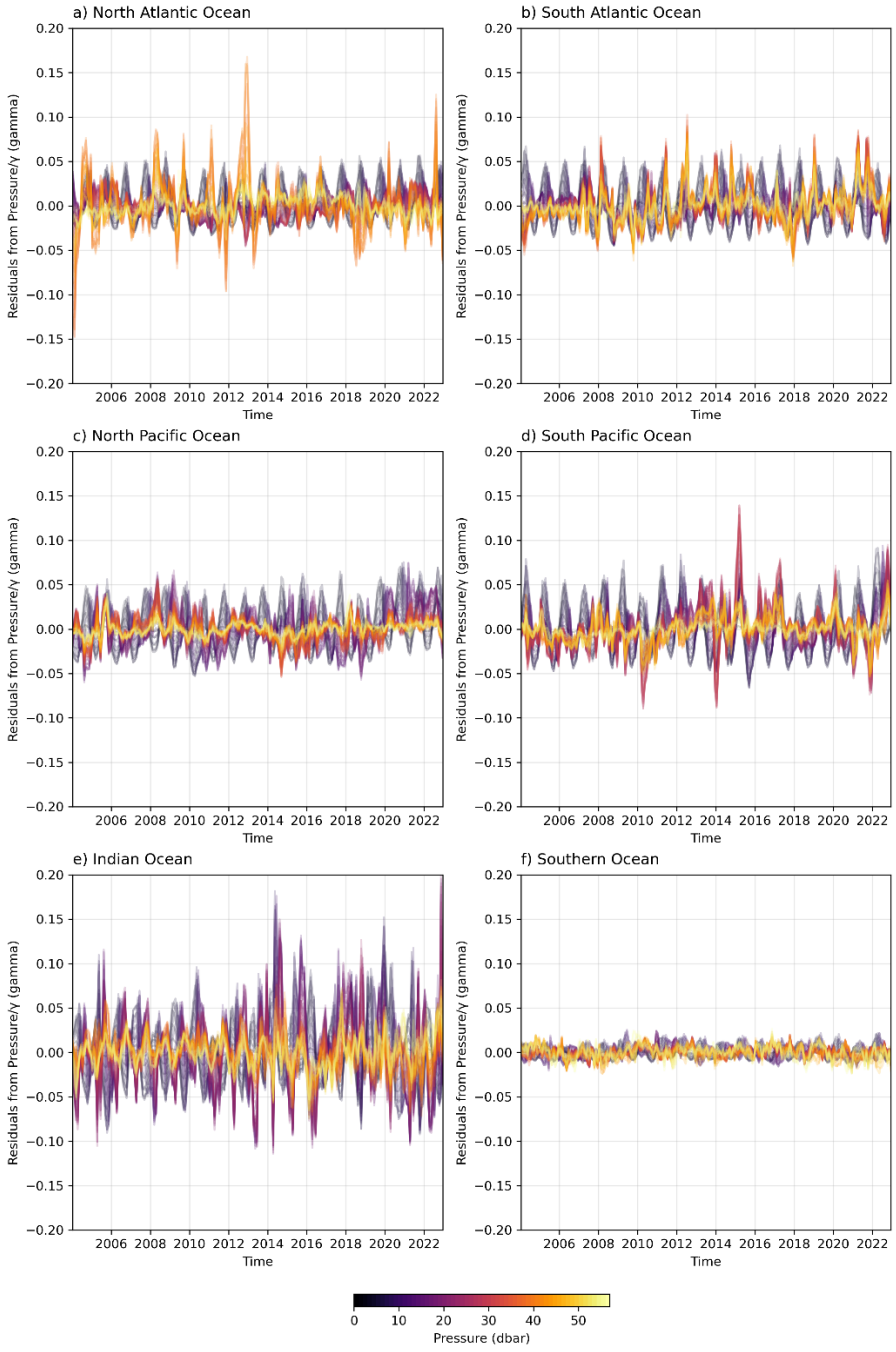

Figure S5. Residuals from the mean pressure/γ (gamma) ratio across all pressure levels from the 4D synthetic dataset over time for each ocean basin. The residuals are calculated for the North Atlantic Ocean (a), South Atlantic Ocean (b), North Pacific Ocean (c), South Pacific Ocean (d), Indian Ocean (e), and Southern Ocean (f). Each line represents the deviation of the pressure/γ (gamma) ratio from the mean ratio at a given pressure level (indicated by the color gradient) over the time series. The pressure/γ (gamma) ratio provides a normalized measure of the relationship between pressure and neutral density at each level, used here to assess whether significant shifts in water mass structure (e.g., due to heave) have occurred over time.

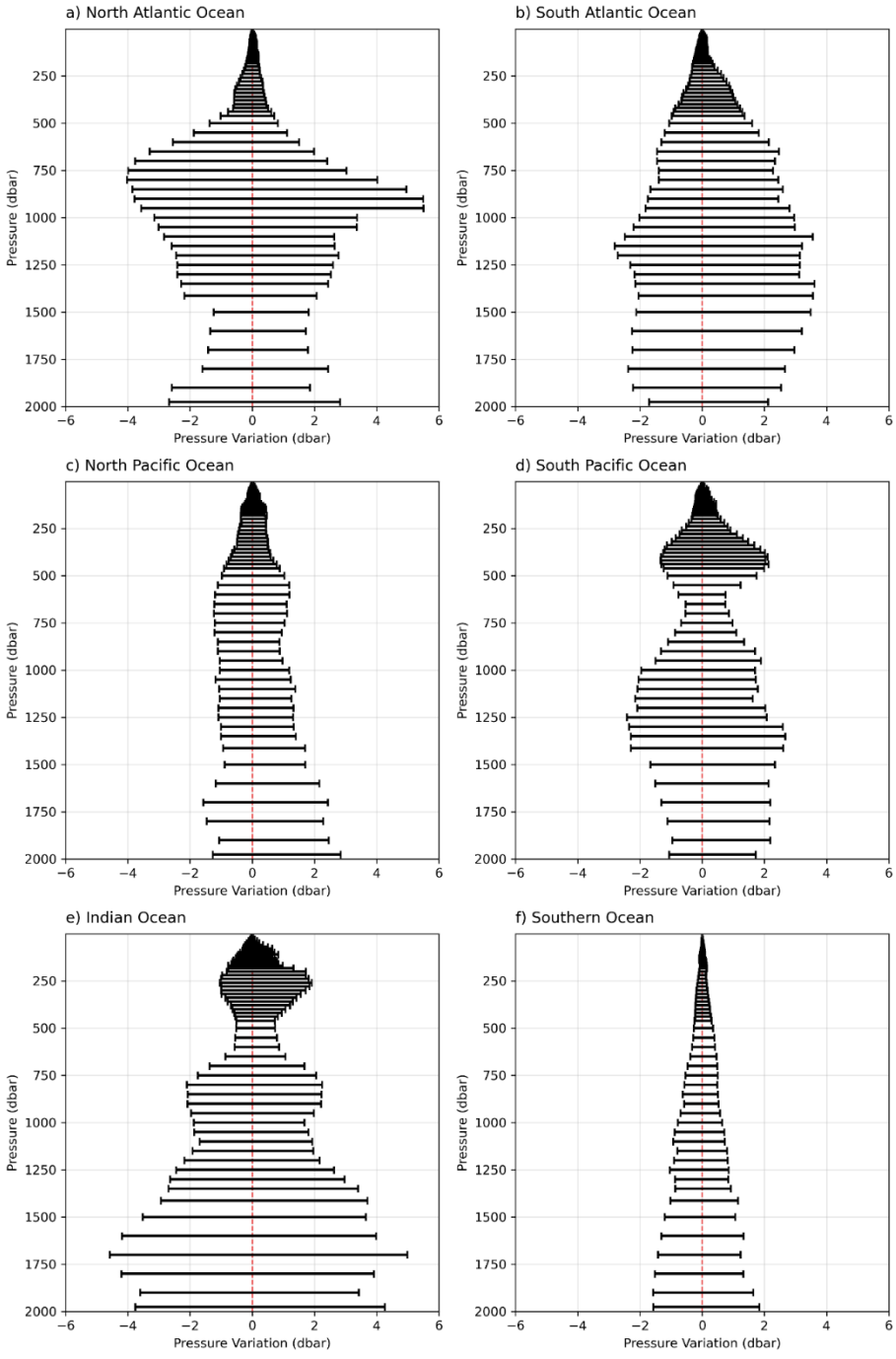

Figure S6. Range of pressure variations at each depth level across major ocean basins, derived from the 4D GCC-DIC dataset. Each horizontal line shows the minimum and maximum pressure deviation from the long-term mean, calculated for each pressure level over the 2004–2022 period. Panels correspond to the North Atlantic (a), South Atlantic (b), North Pacific (c), South Pacific (d), Indian (e), and Southern (f) Oceans. These variations reflect how much pressure at a given depth level differs from the neutral density surface over time. The red dashed line at x = 0 indicates no deviation from the mean.

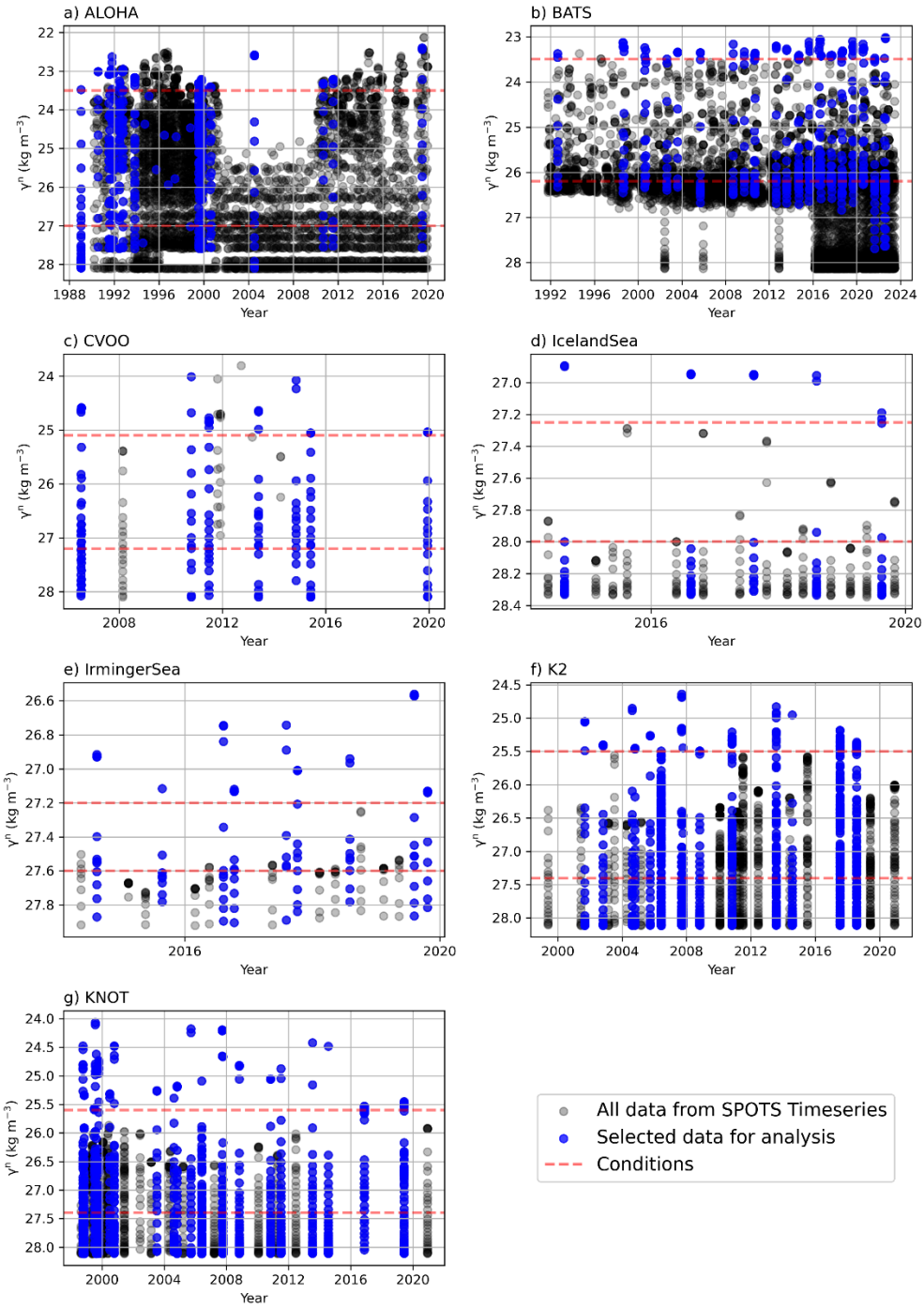

Figure S7. Independent time series analyses from the SPOTs compilation, displaying profiles through time for selected sites. Each subplot represents a unique site where profiles have been selected based on a predefined minimum and maximum neutral density. This selection criterion ensures consistent analysis across all sites for observing changes in the components DIC through time. All data are shown in black and selected data points in blue. Red dashed lines indicate the boundaries set by the minimum and maximum neutral density values.

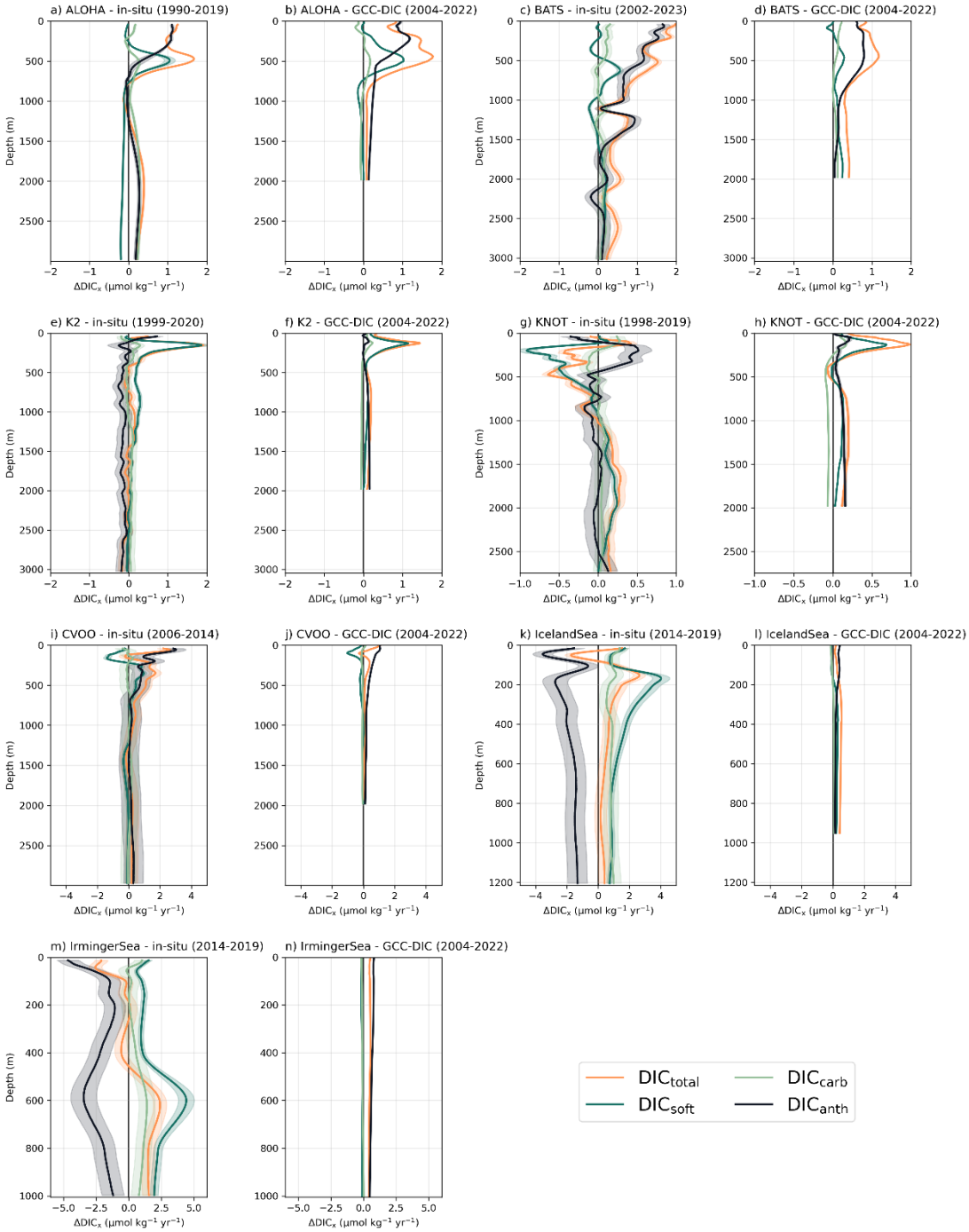

Figure S8. Changes in DIC and its components at selected independent ocean time series sites. Each subplot shows the in situ rate of change over the full observational period (black, with shading for uncertainty) and the corresponding trend from the GCC-DIC reconstruction for 2004–2022, decomposed into total DIC_{total} (orange), DIC_{soft} (green), DIC_{carb} (light green), and DIC_{anth} (dark grey). Overall, GCC-DIC aligns with the direction and structure of observed trends at most sites, though regional discrepancies exist — notably in the Irminger and Iceland Seas — which may reflect the limited duration of some time series or the timing of trend emergence (Henson et al., 2016). In the Irminger Sea, for example, the decrease in $DIC_{soo}f$ observed in GCC-DIC is consistent with previous findings (Fröb et al., 2018), suggesting that the short in situ record may not yet capture the longer-term trend.

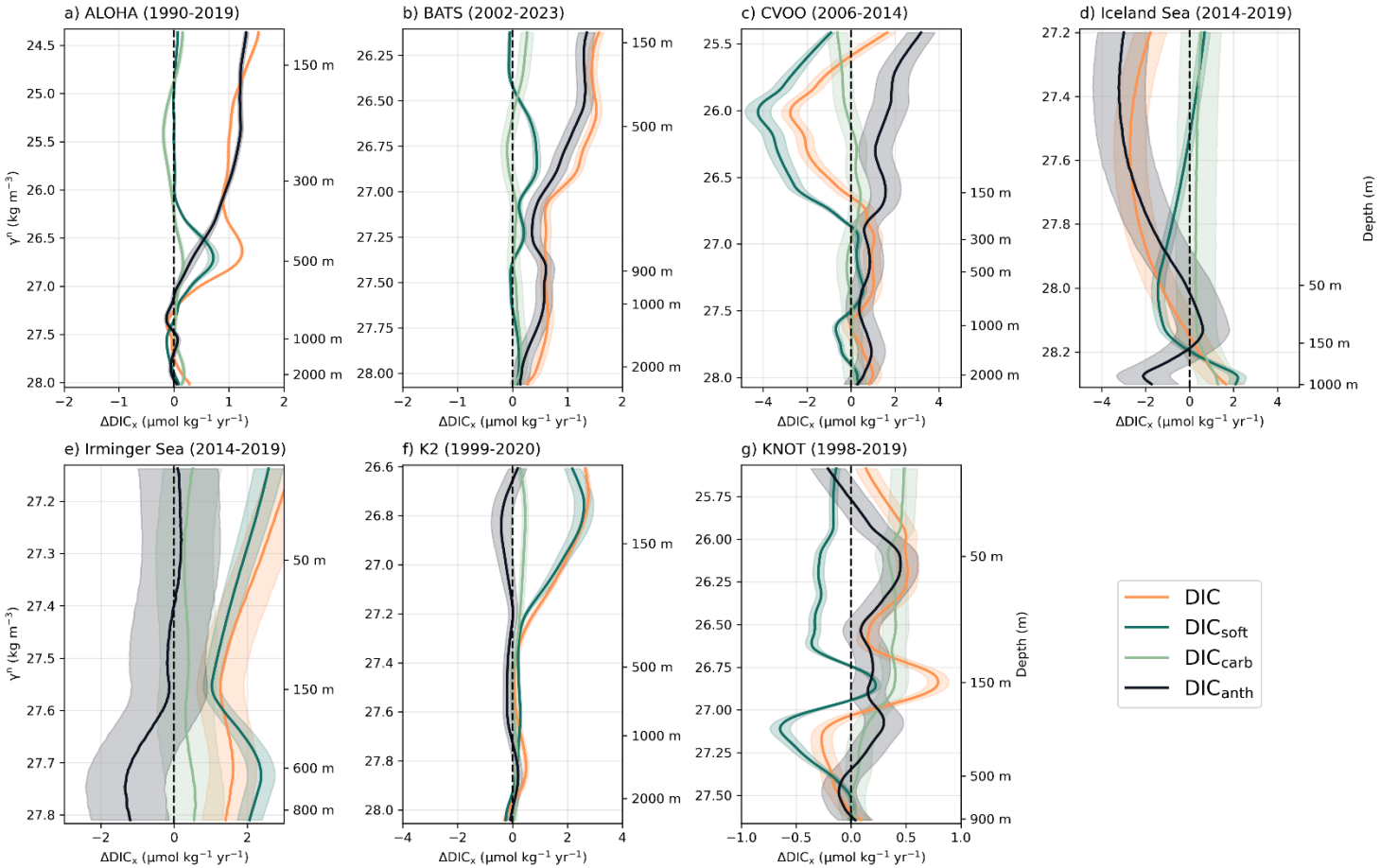

Figure S9. Same analysis as Figure S7 but in neutral density space, which more closely follows isopycnal surfaces and better accounts for water mass movement than fixed-depth coordinates. Approximate depths are shown. While neutral density space offers a more physically consistent framework for following water mass trajectories, our parallel analysis (see Methods, Fig. S3–S5) showed that pressure space remains a valid and practical choice, with vertical deviations due to heave remaining small (~6 dbar) and lacking long-term trends. Accordingly, pressure-based analysis (used in the main text) is sufficient for capturing decadal variability in DIC components.

Station	Sequestration depth trend (m year-1)	Trend significance (p-value)	Change in sequestration depth (m)	Change significance (p-value)	Late 50% sequestration depth (m)
ALOHA	-0.51 ± 0.019	< 0.05	-13.3 ± 0.67	< 0.05	1611
BATS	1.8 ± 0.31	< 0.05	24.5 ± 2.2	< 0.05	1449
CVOO	-1.5 ± 1.9	> 0.05	-10.5 ± 9.7	> 0.05	1102
Iceland Sea	-5.8 ± 0.32	< 0.05	-24.5 ± 1.4	< 0.05	728
Irminger Sea	-8.5 ± 1.3	< 0.05	-30.3 ± 6.1	< 0.05	739
K2	-0.96 ± 0.20	< 0.05	-11.7 ± 3.1	< 0.05	1432
KNOT	1.0 ± 0.15	< 0.05	11.3 ± 3.4	< 0.05	1383

Table S2. Statistical trends in the depth at which 50% of DIC_{soft} is sequestered across in-situ time series stations. The slope (m $year^{-1}$) represents the rate of change in sequestration depth over time while the change in sequestration depth (m) quantifies the difference in sequestration depth between the mean first (Q1) and mean fourth (Q4) quartiles. The late 50% sequestration depth represents the mean 50% sequestration depth of Q4. Note that all statistics were significant except at station CVOO, likely due to too few observations.

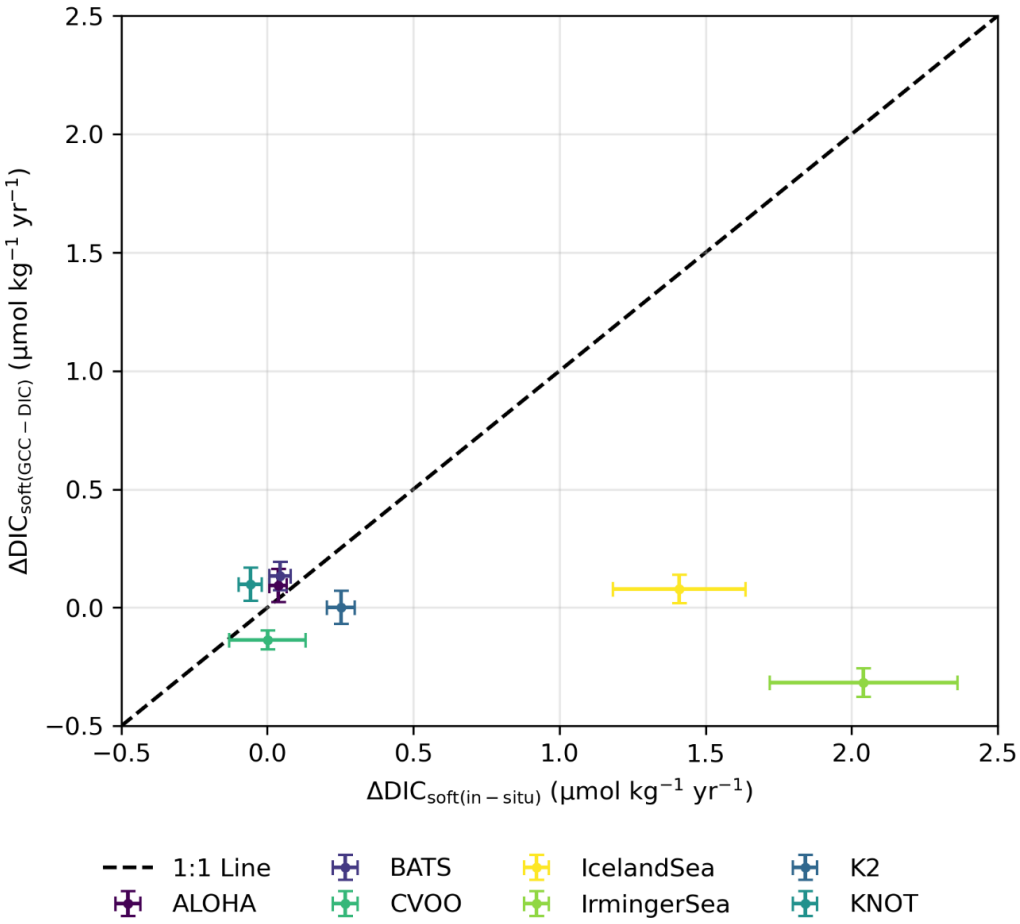

Figure S10. Comparison of in-situ time series and GCC-DIC depth-weighted changes in DIC_{soft}. Error bars represent propagated uncertainties: horizontal bars for in-situ observations and vertical bars for modeled GCC-DIC data. In some cases, the in situ time series show larger uncertainties than the reconstruction, particularly in the Irminger and Iceland Seas. This likely reflects the limited number of observations and shorter time coverage at these sites, which reduce the statistical robustness of the trend estimates compared to the gridded and temporally complete GCC-DIC product.

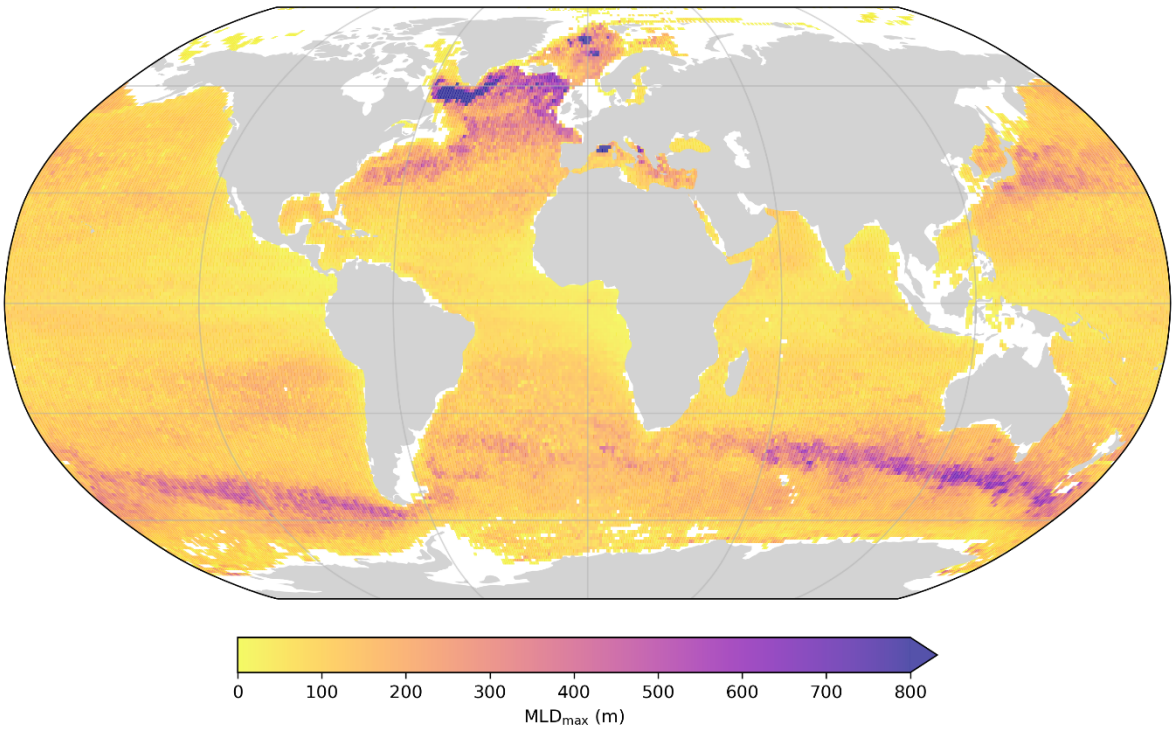

Figure S11. Spatial distribution of the maximum mixed layer depth (MLD) across the global ocean, based on the Argo mixed layer climatology developed by Holte et al. (2017). The MLD values represent the maximum monthly climatological depths determined using a hybrid density algorithm, applied to over 2.6 million Argo profiles collected between 2000 and 2021. The climatology used here is the most recent version, updated in April 2022. The maximum MLD is defined as the mean of the three deepest MLDs in each 1° × 1° grid cell. This climatology provides a physically consistent estimate of the deepest annual mixing, relevant for evaluating vertical exchange and potential carbon sequestration.

Scenario	Full sample					20% sample				
	n profiles	Mean WD	Min WD	Max WD	σ_1 WD	n profiles	Mean WD	Min WD	Max WD	σ_1 WD
↑ DIC_{soft} ↑ 50% depth	8616	2.8	0.03	19.0	1.9	1723	2.8	0.05	17.8	2.0
↓ DIC_{soft} ↓ 50% depth	2445	3.3	0.06	18.0	2.3	489	3.5	0.08	18.0	2.5
↑ DIC_{soft} ↓ 50% depth	14054	3.8	0.03	24.9	2.5	2810	3.9	0.07	24.1	2.7
↓ DIC_{soft} ↑ 50% depth	5363	3.6	0.03	23.5	2.4	1072	3.5	0.06	17.4	2.3

Table S3. Summary of pairwise Wasserstein distances (WD) between residual DIC_{soft} profiles within each scenario. Residuals were defined as the difference between the full annual DIC_{soft} profiles from the years of maximum and minimum total DIC_{soft} below the mixed layer, at each pixel. The WD, in units of μmol m kg^{-1}, quantifies the amount of vertical redistribution required to transform one profile into another. The four scenarios represent different combinations of long-term sequestration change (ΔDIC_{soft} below MLD; Fig. 3a) and sequestration depth change (trend in 50% sequestration depth; Fig. 3b): (1) more carbon stored at depth, and deepening; (2) less carbon stored, and shoaling; (3) more carbon stored, but shoaling; and (4) less carbon stored, but deepening. Both full datasets and 20% random subsamples are shown. Across all scenarios, mean WD values remained consistent between full and subsampled sets (differences <0.2 μmol m kg^{-1}), indicating robust internal similarity within each scenario. Mean WD values ranged from 2.8 to 3.9 μmol m kg^{-1}, suggesting that only minor vertical redistributions of carbon are needed to align profiles within each quadrant, despite spanning thousands of global grid points.

References

Lange, N., Fiedler, B., Álvarez, M., Benoit-Cattin, A., Benway, H., Buttigieg, P. L., Coppola, L., Currie, K., Flecha, S., Gerlach, D. S., Honda, M., Huertas, I. E., Lauvset, S. K., Muller-Karger, F., Körtzinger, A., O'Brien, K. M., Ólafsdóttir, S. R., Pacheco, F. C., Rueda-Roa, D., . . . Tanhua, T. (2024). Synthesis Product for Ocean Time Series (SPOTS) – a ship-based biogeochemical pilot. *Earth Syst. Sci. Data*, *16*(4), 1901-1931. https://doi.org/10.5194/essd-16-1901-2024

Fröb, F., Olsen, A., Pérez, F. F., García-Ibáñez, M. I., Jeansson, E., Omar, A., & Lauvset, S. K. (2018). Inorganic carbon and water masses in the Irminger Sea since 1991. *Biogeosciences*, *15*(1), 51-72. https://doi.org/10.5194/bg-15-51-2018

Henson, S. A., Beaulieu, C., & Lampitt, R. (2016). Observing climate change trends in ocean biogeochemistry: when and where. *Global change biology*, *22*(4), 1561-1571.

Holte, J., Talley, L. D., Gilson, J., & Roemmich, D. (2017). An Argo mixed layer climatology and database. *Geophysical Research Letters*, *44*(11), 5618-5626. https://doi.org/https://doi.org/10.1002/2017GL073426